Dalton Transactions

PAPER

View Article Online
View Journal | View Issue

Cite this: *Dalton Trans.*, 2019, **48**, 9117

Anionic guest-dependent slow magnetic relaxation in Co(II) tripodal iminopyridine complexes†

Christina M. Klug,‡ Tarik J. Ozumerzifon, § Indrani Bhowmick, ¶ Brooke N. Livesay, Anthony K. Rappé and Matthew P. Shores *

Received 18th February 2019,
Accepted 24th February 2019

DOI: 10.1039/c9dt00739c

rsc.li/dalton

We report the syntheses and magnetic property characterizations of four mononuclear cobalt(II) complex salts featuring a tripodal iminopyridine ligand with external anion receptor groups, $[CoL^{5\text{-}ONHtBu}]X_2$ (X = Cl (**1**), Br (**2**), I (**3**) and ClO_4 (**4**)). While all four salts exhibit anion binding through pendant amide moieties, only in the case of **1** is field-induced slow relaxation of magnetisation observed, whereas in the other salts this phenomenon is absent at the limits of our instrumentation. The effect of chloride inducing a seventh Co–N interaction and concomitant structural distortion is hypothesized as the origin of the observed dynamic magnetic properties observed in **1**. *Ab initio* computational studies carried out on a 7-coordinate Co(II) model species survey the complex interplay of coordination number and trigonal twisting on the sign and magnitude of the axial anisotropy parameter (*D*), and identify structural features whose distortions can trigger large switches in the sign and magnitude of magnetic anisotropy.

Introduction

Efforts to control the switching of magnetic properties at the molecular level have advanced the feasibility of devices for nanoscale data storage, actuators and sensors. Magnetic bistability exhibited by single-molecule magnets (SMMs) may also be exploited in molecular switching applications. For instance, reports have shown first row transition metal complexes that can switch between spin crossover and SMM properties.[1–5] Other cases have shown magnetic relaxation profiles in SMMs can be modulated by intermolecular interactions. This phenomenon is sensitive to guest and/or solvent inclusion in both molecular systems[6–10] and extended structures, such as metal–organic framework materials.[11,12] Herein, we describe a complex architecture where anionic guest binding far from the metal centre nevertheless imparts a strong effect on magnetic relaxation dynamics.

To further develop the field of guest-dependent magnetic switching in molecular species, we have focused on complexes with tripodal iminopyridine ligands that contain anion-receptors. Related tris(2-aminoethylamine) (tren)-derived species have been shown to possess sterically-tuned spin crossover properties;[13–15] further, the hexa- or heptadentate coordination environment might be expected to promote complex stability in solution. Specifically, we have found that Fe(II) complexes with tren-capped iminopyridine ligands, where anion-binding groups are installed at the pyridine 5-position and steric bulk is absent at the 6-position (Fig. 1, right), are low spin ($S = 0$)

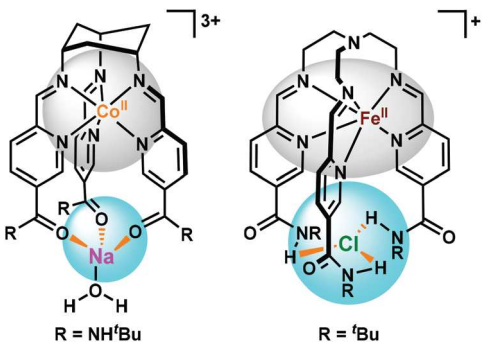

Fig. 1 Differences in metal and guest binding pockets between previously reported tach- and tren-based M(II) podands. Gray and blue circles represent metal and guest binding pockets, respectively. The tach-containing pocket (left) enforces hexacoordinate geometries, while the tren-based ligand (right) allows for hexa- and hepta-coordinate geometries.

Department of Chemistry, Colorado State University, Fort Collins, CO 80523, USA. E-mail: matthew.shores@colostate.edu

† Electronic supplementary information (ESI) available: Details of magnetic and computational studies. CCDC 1030387–1030390 for **1–4**. For ESI and crystallographic data in CIF or other electronic format see DOI: 10.1039/c9dt00739c

‡ Current affiliation: Pacific Northwest National Laboratory, Richland, WA 99352, USA.

§ Current affiliation: Isola Group, Chandler, AZ 85224, USA.

¶ Current affiliation: Colorado State University, Pueblo.

irrespective of guest presence.[16] Nevertheless, the complexes show chloride binding in polar (acetonitrile) solution.

In contrast, related ligand sets bound to Co(II) yield high spin ($S = 3/2$) ground states. These ions have been incorporated into a growing number of mono- and polynuclear SMM complexes,[17–19] as the intrinsically large spin–orbit coupling value for Co(II) gives rise to significant zero-field splitting (ZFS).[20–22] Ligand distortion of the first coordination sphere of the Co(II) ion has large impacts on axial (D) and rhombic (E) anisotropy parameters.[9,22,23] In a related example, our recently reported *cis*-,*cis*-1,3,5-triaminocyclohexane (tach)-capped Co(II) tripodal complex (Fig. 1, left) displays unusual cationic guest association and slow magnetic relaxation.[24] However, we also found that the inherent rigidity of the tach-based scaffold renders the complex coordination environment around cobalt insensitive to guest association.

Therefore, to modulate the magnetic properties of Co(II) podand complexes *via* guest inclusion, we have implemented a more flexible ligand cap derived from tren (Fig. 1, right). In the present work, the syntheses and magnetic characterizations of a series of Co(II) complex salts are reported, where the results suggest turn-on magnetic relaxation as a function of guest anion. To tease apart the key structural factors that drive the magnetic switching, we also report the results of an in-depth computational investigation of the effects of introducing a seventh ligand into a face-capped octahedral system.

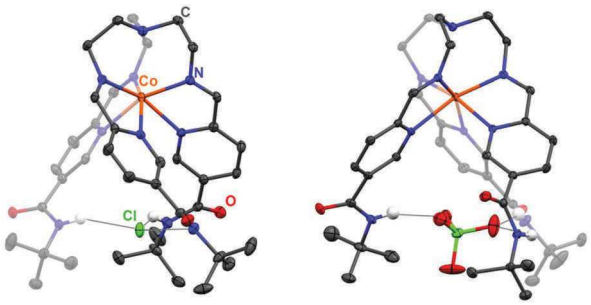

Fig. 2 Crystal structures of the complex cations of **1** (left) and **4** (right) depicted with 40% thermal ellipsoids. Orange, green, red, blue, gray and white ellipsoids represent Co, Cl, O, N, C and H atoms, respectively. Hydrogen atoms not involved in hydrogen bonding and unbound anions have been omitted for clarity. The structure for **1** resides on a three-fold rotation site, while the complex for **4** sits on a general position.

Results and discussion

Complex salt syntheses and anion-binding properties

The compounds $[CoL^{5\text{-}ONHtBu}]X_2$ (where X = Cl (**1**), Br (**2**), I (**3**), or ClO_4 (**4**)) are synthesized by combining the respective CoX_2 starting material and tripodal iminopyridine $L^{5\text{-}ONHtBu}$ in methanol. Diffusion of diethyl ether into concentrated crude reaction mixtures (as methanolic solutions) readily affords diffraction-quality orange crystals of the four salts. The halide salts **1–3** crystallize in the trigonal space group $P\bar{3}$, whereas the perchlorate salt **4** crystallizes in $P\bar{1}$. The first coordination spheres of the metal centres show the expected N_6 environment in a distorted octahedron (Fig. 2 and S1†), capped on one face by the bridging nitrogen atom from the tren backbone (N_{bridge}, Table 1) providing a pseudo-heptacoordinate environment around the Co(II) centre. As shown in Table 1, the Co–N_{imine} bonds (average 2.108(3) Å) in **1–4** are shorter than the Co–$N_{pyridine}$ bonds (average 2.255(1) Å), consistent with previously reported iminopyridine-based first row transition metal complexes.[13,25,26] The degree of distortion from an ideal capped octahedron was measured using the continuous shape measurement analysis using the SHAPE 2.0 software.[27,28] The afforded values were found to be between 1.18–1.49, suggestive of a distorted capped octahedron coordination geometry for all four complexes.

For salts **1–4**, one anion is encapsulated within the trigonal pocket formed by the three *tert*-butylamide functionalities of the ligand. The area of the triangular pocket formed by the carbon atoms of the amide carbonyl in the halide series ranges from 19.03(1) $Å^2$ in **1** to 21.89(6) $Å^2$ in **3** (Table S2†), highlighting the increased flexibility of the tren capping ligand. In comparison, the same areas measured for the more rigid tach analogues vary only between 13.40(3) and 14.38(6) $Å^2$.[24]

Given the isotropy of the halide guests, it is not surprising that the interactions with the arms are similar, which leads to three-fold symmetry of the complex cation. In comparison, the asymmetry of the bound perchlorate in **4** makes these interactions distinct: one oxygen of the perchlorate engages in a bifurcated hydrogen bond with two amides while another oxygen engages in a hydrogen bond to the third arm of the ligand; the third oxygen atom in the "trigonal" pocket does not interact with amide hydrogen atoms. In fact, the structure of **4** is distinct from **1–3** in that the three amide N–H groups

Table 1 Selected crystallographic parameters

	1	2	3	4	$[CoL^{5\text{-}OOMe}][CoCl_4]$[a]
Co–N_{bridge} (Å)	2.574(3)	2.592(4)	2.633(6)	2.706(2)	2.6262(2)
Co–N_{im}[b] (Å)	2.120(6)	2.106(6)	2.105(3)	2.100(5)	2.079(1)
Co–N_{py}[b] (Å)	2.262(3)	2.253(3)	2.258(3)	2.246(5)	2.228(1)
im-py dist[c] (Å)	2.099(2)	2.092(3)	2.068(4)	2.075(2)	2.068(2)
φ[d] (°)	49.8(4)	50.5(3)	51.3(6)	51.2(9)	50.4(6)
Σ (°)	125.9(3)	120.4(4)	117.9(5)	113.3(2)	123.3(1)
SHAPE value	1.18	1.23	1.30	1.49	1.27

[a] Structure where methyl ester replaces the amide group; from ref. 21. [b] Average distance for **4**. [c] Distance between the planes defined by the imine and pyridine nitrogen atoms, respectively. [d] Trigonal twisting angle of 0° gives a trigonal prism, while 60° gives an octahedron.

are not oriented toward the molecular three-fold axis (Fig. 2, right).

The packing of salts **1–3** results in the formation of channels within the structure, which contain severely disordered solvent molecules and the remaining charge balancing anion. The intermolecular Co···Co distances range from 8.003(8) Å in **4** to 9.480(9) Å in **3**. For salts **1–3**, the packing and longer intermolecular distances effectively isolate the complexes from each other. However, in **4**, short intermolecular contacts are present between the perchlorate bound within the trigonal pocket and the tren ethylene backbone of an adjacent cation (Fig. S2†), forming supramolecular chains. These interactions may provide pathways for intermolecular magnetic exchange.

Whereas the geometry of the tach-containing analogue of **1–4** is insensitive to guest inclusion, we may expect more guest-induced ligand distortion from the larger tren capping group. Salts **1–4** crystallized with an anion contained in the tris(amide) pocket. Notwithstanding, structural comparison to the previously reported[25] ester-containing analogue, which does not contain a guest in the trigonal pocket, reveals the anticipated geometric flexibility (Table 1). Interestingly, the presence or absence of guest anions does not significantly change the trigonal twisting in the Co(II) complexes. For the ester-containing analogue, the interaction between Co and the seventh ligand (Co–N_{bridge} distance) is in the middle of the range provided by compounds **1–4** (Tables 1). Additionally, the imine-pyridine interplane distance is as short or shorter than all of the amide-containing structures, signalling elongation upon anion binding. These distance changes highlight the flexibility of the tren backbone to respond to guest species.

Complex salt magnetic properties

Temperature dependent magnetic susceptibility data for **1–4** (Fig. 3 and S10–S13†) indicate that all species are high spin (S = 3/2) over the temperatures probed. At 300 K, the $\chi_M T$ values are 2.96, 2.84, 3.02 and 2.92 cm^3 K mol^{-1} for compounds **1–4**, respectively; larger than the expected spin-only value (1.875 cm^3 K mol^{-1}), but consistent with observations for many Co(II) complexes.[23] The $\chi_M T$ products of all species decrease gradually upon cooling from 300 to 50 K. For the halide-bound salts, significant downturns below 50 K are observed; these are attributed to magnetic anisotropy and/or intermolecular antiferromagnetic interactions. For the perchlorate salt **4**, the $\chi_M T$ value increases between 50 K and 8 K, to 2.49 cm^3 K mol^{-1}, before decreasing like the others, suggesting additional intermolecular ferromagnetic interactions. Salts **1–4** show $\chi_M T$ values of 1.52, 2.03, 1.59, and 2.04 cm^3 K mol^{-1} at 2 K, respectively, consistent with anisotropic quartet ground states.

Fitting the magnetic susceptibility data to standard spin Hamiltonians with PHI[29] also supports anisotropic quartet ground states for all four salts (Tables 2 and S3†). We note that the sign of the axial anisotropy parameter is not reliably determined from susceptibility data, but the positive signs are consistent with fits to the reduced magnetization data. A small positive mean field contribution is included in the fits of **1** and **4**, suggesting weak antiferro- and ferromagnetic interactions between complexes (zJ = −0.099 and 0.028 cm^{-1}, for **1** and **4** respectively), possibly arising from short intermolecular contacts noted in the structural studies; ferromagnetic intermolecular coupling mediated by hydrogen-bonding interactions has been reported for Co(II)-containing compounds previously.[30]

We note that the reduced magnetisation data obtained for salts **1–4** (Fig. S14†) also support the assignment of S = 3/2 ground states for all complex salts. These data were fit in tandem with susceptibility data using PHI.[29] The results are consistent with the magnetic behaviour of the perchlorate salt of the ester-containing analogue,[25] and indicate that the geometric changes upon interaction with anions are too small to impact spin state properties.

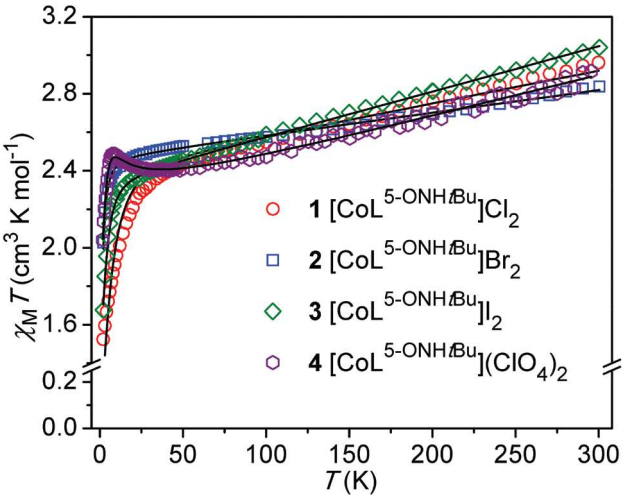

Fig. 3 Variable temperature dc magnetic susceptibility data for **1–4** collected between 1.8 and 300 K at an applied field of 1000 Oe. The fit lines were determined using PHI[29], with the parameters obtained found in Table 2. Individual figures for **1–4** can be found in the ESI.†

Table 2 Comparison of magnetic parameters obtained from fits to magnetic susceptibility data (PHI)[29] and CASCI computations

	Experiment[a]			Computation		
Salt	g_x, g_y, g_z	D^b	$\lvert E/D\rvert$	g_x, g_y, g_z	D^b	$\lvert E/D\rvert$
1	2.31, 2.39, 2.10	9.20	0.002	2.18, 2.30, 2.30	9.8	0.03
2	1.87, 2.56, 2.39	2.19	<0.001	2.18, 2.30, 2.30	5.9	0.010
3	2.14, 2.25, 2.32	3.61	0.399	2.17, 2.31, 2.32	12.4	0.006
4	3.55, 0.75, 1.04	4.21	0.060	2.16, 2.34, 2.34	15.9	0.002

[a] Although fits to reduced magnetization do not reliably give signs for D, the experimental and computational signs agree here; see Table S4 for details. [b] D values given in cm^{-1}.

Anion dependence in SMM properties

While the extracted anisotropy parameters are modest relative to many mononuclear Co(II) SMMs, we observe an interesting

anion dependence in this series. Chloride salt **1** has a (relatively) larger axial anisotropy D value than the other salts, and axiality (minimization of E/D) is strongest in the chloride and bromide salts. Testing salts **1–4** for SMM properties, we note that none of the salts display out-of-phase susceptibility (χ'') responses under zero applied dc field at 1.8 K. Upon application of an external dc field, however, chloride salt **1** exhibits slow relaxation of magnetisation (Fig. 4), where the χ'' signal is maximized at 2500 Oe (Fig. S16 and S17†).

The bromide salt **2** displays a negligible out-of-phase response even with the application of a dc field up to 5000 Oe (Fig. S18†). Meanwhile, the iodide (**3**) and perchlorate (**4**) salts show slight increases in the out-of-phase magnetic susceptibilities under applied dc field at higher frequencies (Fig. S19 and S20†), but do not produce maximum responses within the frequency limits of our instrument. Further, the perchlorate salt of the analogous ester-containing complex also does not exhibit slow relaxation at the limits of our measurement (Fig. S23,† H_{dc} = 2500 Oe). The local coordination geometry of the [CoL$^{5\text{-OOMe}}$] complex in the tetrachlorocobaltate salt[25] is most comparable to the anion-bound species **3** and **4**, which also do not show slow relaxation even under applied dc fields.[31]

The temperature and frequency dependencies of the ac magnetic susceptibility were studied for **1** under an applied dc field of 2500 Oe, with a 4 Oe oscillating ac field, for a range of temperatures (1.8–4.6 K). Maxima in the χ'' data are observable between 1.8 and 3.0 K (Fig. 5), and can be fit to an Orbach-only relaxation process, where $\tau^{-1} = \tau_0^{-1}\exp(-U_{eff}/kT)$. This treatment gives $\tau_0 = 1.33 \times 10^{-6}$ s and $U_{eff} = 9.2$ cm^{-1} (Fig. S21†). The thermal barrier (U_{eff}) and pre-exponential constant (τ_0) are consistent with other seven-coordinate Co(II) SMMs.[32–37]

The exhibition of field-induced slow magnetic relaxation for **1** is concurrent with it being the most axially anisotropic of the four salts and possessing the largest magnitude axial anisotropy. Because the halide salts are isostructural, intermolecular interactions are unlikely to be the source of this distinction. A caveat is that all three halide-containing salts show extensive disorder in the one-dimensional channels formed by packing, including the second charge-balancing anion, so we cannot completely rule out differences in supramolecular environments for the complexes. Notwithstanding, we note subtle but significant differences in local Co(II) geometry owing to the different anions interacting with the complex. The change in ionic radius going from chloride (184 pm) to bromide (196 pm) to iodide (220 pm) enlarges the ligand pocket, distorting the cobalt coordination sphere. It has been shown that altering the geometry around a Co(II) centre can alter relaxation properties,[20,22] so this may enable pathways for fast magnetic relaxation for **2–4**, which are inaccessible for **1**.

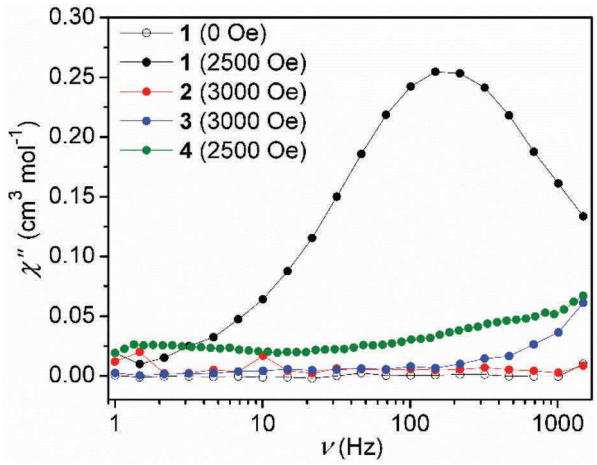

Fig. 4 Frequency dependence of the out-of-phase susceptibility for **1–4** at listed applied dc fields. Data were collected at 1.9 K using a 4 Oe oscillating field. Lines are guides to the eye.

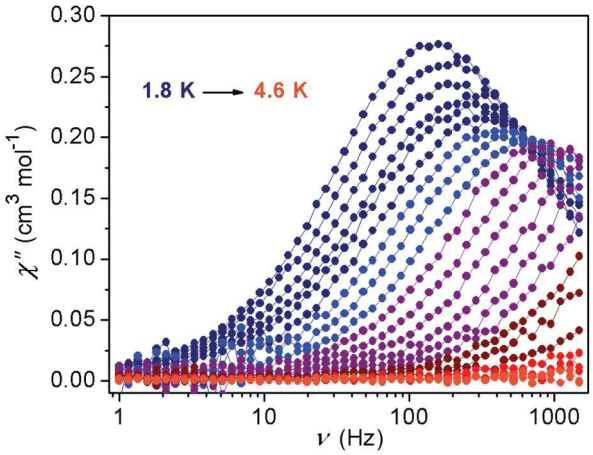

Fig. 5 Variable frequency out-of-phase ac susceptibility for **1**, collected at a 2500 Oe applied dc field, with a 4 Oe ac oscillating ac field, in the temperature range 1.8 to 4.6 K. Data were collected at 0.1 K increments from 1.8 K to 3.4 K and at 0.2 K increments from 3.6 to 4.6 K.

Focusing on the halide salts, two observable crystallographic trends are the compression of the N-donor atom planes along the 3-fold trigonal axis (Table 1), and an increase in Co–N$_{bridge}$ distance from the chloride to bromide to iodide salt. The ester-containing analogue, the closest proxy available for non-binding by anion, adds to the former trend with an even shorter imine-pyridine interplane distance. These structural trends coincide with a decrease in experimentally-derived axiality (E/D) as halide size increases. Comparison to other C_3-symmetric Fe(II) and Co(II) species employing tripodal ligands capped by a nitrogen atom show that an increase in M–N$_{bridge}$ distance leads to a decrease in the magnitude of D, with concomitant effects on SMM properties.[38–40] In our system, chloride salt **1** has the shortest Co–N$_{bridge}$ distance and is the only compound that shows field-induced slow magnetic relaxation.

Computational exploration of ligand distortion effects on Co(II) magnetic anisotropy

Whereas the experimental data suggest magnetic property control *via* steric interactions, especially in terms of axiality

(E/D), computational results do not provide the same correlation. Computations were carried out at several levels of theory on systems closely related to the experimentally determined structures, and results are summarized in Tables S5–S9.† An important caveat is that anions not located in the tris(amide) binding pockets are severely disordered in the halide-containing structures, so their placement along the 3-fold rotational axis for computations offers consistency and convenience, but also removes rhombic anisotropy by symmetry arguments. Notwithstanding, and not surprisingly, the more resource-intensive NEVPT2[41–44] or CASCI[45] computations give better numerical agreement with measured D values, while density functional (B3LYP)[46] calculations give $|D|$ values about half of what are measured. However, the trends are similar with all sets of computations. For example, in both cases, the Br-containing salt is expected to show the least axiality (largest E/D), the iodide salt should show the largest magnitude of D for the halides, and the perchlorate salt should show the largest $|D|$ value within the family. As expected, all computed values suggest minimal rhombic anisotropy. We attribute this to the placement of the second anion, which promotes 3-fold rotational symmetry and minimizes E. For this reason, we will focus on the axial component D in the remaining discussion.

CASSCF, NEVPT2, and CASCI give excited state energies about half of what is computed *via* TD-DFT[47] methods (Table S9†). The more compressed manifold of excited states leads to larger anisotropy, but the signs of the anisotropy parameters are opposite and tend to cancel each other out, leading to small overall anisotropies. This is similar to what Dunbar and coworkers reported for 5-coordinate complexes,[9] at least in terms of competing large anisotropy terms.

Whereas the present set of Co(II) complexes display small positive anisotropies, the recent literature provides many examples of Co(II) species with large $|D|$. As we have shown previously for model $[Co(NH_3)_6]^{2+}$ model complexes,[24] the axial anisotropy parameter for hexacoordinate Co(II) complexes tends to either be near −100 or +100 cm^{-1}, depending upon the extent of trigonal distortion.

These results lead us to computationally investigate the role of a seventh coordination site on the magnetic anisotropy of these and related species using $[Co(NH_3)_7]^{2+}$ as a model. In this system, we varied the distance (R) of a seventh ammine ligand for various trigonal distortion angles. Here, we employed the effective spin Hamiltonian CASSCF/NEVPT2 or CASSCF/CASCI methods[41–44,48,49] which has been used previously by us[24,33] and others[50–55] for evaluation of magnetic anisotropy in Co(II) systems. As pointed out previously[56] this approach is potentially problematic for systems with low-lying excited states. The CASCI results for D are shown in Fig. 6. Computed g values are provided as supplementary figures in the ESI (Fig. S24b–d†). We note that alternative methods for establishing structural distortion impacts on anisotropy may also be effective but are outside the scope of this paper.[57,58]

Previously, Ruiz and co-workers[22] predicted that capped octahedral d^7 complexes should yield small positive D values, while capped trigonal prismatic complexes would yield small negative D values. Here, we find that the sign and magnitude can vary significantly if the seventh Co–L distance (R) is changed. In our previous work,[24] the plus combination of t_{2g} orbitals, labelled dσ, was found to play a significant role in the sign of D. This suggests that a seventh ligand oriented along the three-fold axis would destabilize dσ and could impact D. As can be seen in Fig. 6, when the geometry is more trigonal prismatic in nature (0°, 15°), there is negligible effect on D even as a seventh ligand approaches cobalt. On the other hand, systems with intermediate trigonal twisting (37.5°, 45°) show a pronounced effect as R is altered, where at long distances (4.0 Å), the predicted D values are opposite in sign, but these values nearly converge to a small positive D when R is sufficiently short. The more octahedral systems (52.5°, 60°) exhibit a decrease in D as a function of shortening length, indicating that the role of this parameter is lessened toward the ends of the trigonal distortion spectrum. For the experimentally observed trigonal distortion and seventh ammine distance (R) geometric parameters (2.57 Å–2.71 Å, 50°–51°), the computed D values are small and positive (filled black circles in Fig. 6). These results suggest that the interaction between the seventh ammine and dσ is responsible for the small positive D observed in complex salts **1–4**.

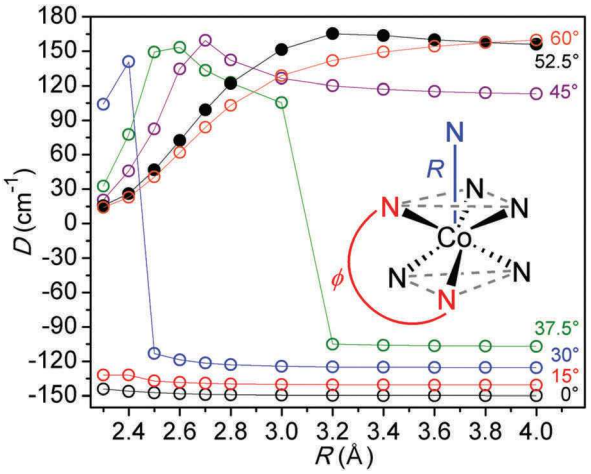

Fig. 6 Calculated D values as a function of seventh Co–N distance (R) at given distortion angles (φ), using face-capped trigonal prismatic $[Co(NH_3)_7]^{2+}$ as a model system. The solid black data points represent the most comparable trigonal distortion to the complex salts **1–4**. Lines serve as guides for the eye.

As would be expected, the rhombic anisotropy parameter E/D is small for octahedral and near trigonal prismatic structures, and maximizes around 38° (Fig. S24a†). There is a pronounced seventh-ligand distance dependence, with the rhombicity decreasing as the seventh ligand approaches. This is consistent with what is observed experimentally, where **1** has the smallest rhombicity.

The trends in g are as expected, based on literature precedent (Fig. S24).† For example, for the Co(II) bis-trispyrazolylborate complex, $g_{\|}$ is large (8.5) and $g_{\perp}$ small (1.0); the CASCI

computed values are 8.54 and 1.38, respectively. For the idealized model $[Co(NH_3)_7]^{2+}$ complex, $g_{\|}$ is 9.82 and $g_{\perp}$ ranges from 0.007 to 0.003 as a function of *R*. As the structure distorts toward octahedral $g_{\|}$ drops to 4.76–4.57. For intermediate angular distortions there is a pronounced seventh-ligand distance dependence.

For intermediate distortions the two smaller components of *g* are not degenerate. The intermediate component smoothly rises with angular distortion while decreasing with increasing *R*. The smallest component initially rises with angle and distance and then decreases with further increase in angular distortion or increasing *R*.

We note that the guide lines connecting data points in Fig. 6 do not connote a simple distortion pathway by which the sign and magnitude of *D* can be switched in the model system. The discontinuities in data for the 30° to 45° degree data likely accrue from limitations of the computational model. The sensitivity of *D* to geometric parameters also suggests that two or more states may be being brought into equilibrium, such that small perturbations (*e.g.* changing cation–anion interactions) might favor one state over another. From the model calculations, the boundary conditions appear to be a seventh ligand in the range 2.5 Å < *R* < 3.0 Å, and a trigonal twisting range of ~20° < ϕ < 40°. Regarding target structures for switching behaviour, the tren-based ligands provide a coordination environment that is more octahedral than desired; nevertheless, relatively minor geometric changes, for example the ~0.05 Å difference between the ester-containing complex and chloride-bound **1**, can combine with other structural factors to allow a switching event. We expect that ligands which drive toward a more trigonal prismatic geometry will enhance the switching: sharp sensitivity of *D* to bond distance shifts of less than 0.1 Å is predicted.

Conclusions

The results presented herein show in detail how small changes in the metal coordination environment can drastically influence dynamic magnetic properties in a Co(II) system. The flexibility of this tren-based iminopyridine ligand allows for expansion of the guest binding pocket and association of anions. The identity of these anionic guests affects not only the magnetic anisotropy of the system, but also the dynamic magnetic properties. This behaviour is most pronounced in the most contracted system **1**, which is the only salt examined here to show slow magnetic relaxation under applied external field. Theoretical considerations have also highlighted the effect of a seventh ligand in a face-capped hexacoordinate Co(II) environment at varying trigonal distortions. While either twisting or seventh ligand compression could promote a magnetic switching event, the available data and computations suggest that anion binding affects seventh ligand location more than trigonal twisting. We are currently developing ligand architectures for host–guest systems that exploit this distortion pathway to perturb spin-state equilibria as well as magnetic anisotropy.

Experimental

General considerations

Unless otherwise noted, all manipulations were performed in a dinitrogen filled MBRAUN Labmaster 130 glovebox. The synthesis and characterization of $L^{5\text{-}ONHtBu}$ has been described elsewhere, but the synthesis of the aldehyde precursor is described in greater detail here (Scheme 1).[16] Acetonitrile (MeCN) and diethyl ether (Et_2O) were sparged with dinitrogen, passed over molecular sieves, and subjected to three freeze–pump–thaw cycles prior to use. All other reagents were obtained from commercial sources and used without further purification unless otherwise indicated. Qualitative thin layer chromatography (TLC) analysis was performed on 250 mm thick, 60 Å, glass backed F254 silica (Silicycle, Quebec City, Canada); samples were visualized with UV light. Flash chromatography was performed using Silicycle silica gel (230–400 mesh).

Magnetic measurements

Magnetic data for **1**, **2** and **4** were collected using a Quantum Design model MPMS-XL superconducting quantum interference device (SQUID) magnetometer. Measurements were collected using crystals of **1**, **2**, and **4** packed into the top of gelatin capsules and restrained with the bottom portion of the capsule. All samples were prepared under a dinitrogen atmosphere and quickly loaded into the SQUID to minimize air exposure. Direct current (dc) susceptibility measurements of crystals of **3** were performed on a Quantum Design model PPMS Dynacool equipped with a VSM transport system. The sample was encased in a polypropylene powder holder prepared under a dinitrogen atmosphere and quickly loaded into the instrument to minimize air exposure. The absence of ferromagnetic impurities was confirmed by observing the linearity of a plot of magnetization *vs.* field at 100 K. In all cases, dc susceptibility measurements were collected from 1.8 K to 300 K under an applied dc field of 1000 Oe. For magnetization experiments, crystals of **1**, **2**, and **4** were encased in six drops of solidified eicosane and crystals of **3** were pressed in a polypropylene powder holder and measured from 1.8 to 30 K under applied dc fields of 1, 2, 3, 4, and 5 T. Data were corrected for

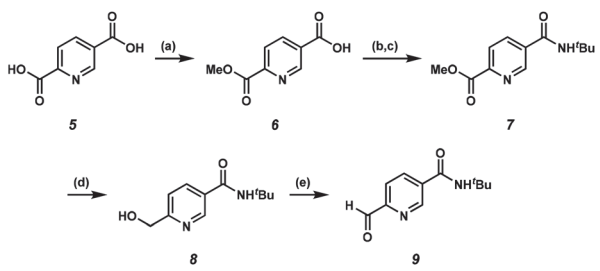

Scheme 1 Synthesis of aldehyde **9**. (a) H_2SO_4 (cat.), MeOH, 70 °C, 75% yield; (b) $SOCl_2$, PhMe, 120 °C; (c) *t*-$BuNH_2$, Et_2O_2, 0 °C; (d) $NaBH_4$, $CaCl_2$, 2 : 1 THF : MeOH, 0 to 23 °C, 85% yield (3 steps); (e) SeO_2, 1,4-dioxane, 101 °C, 75% yield.

the magnetization of the sample holder by subtracting the susceptibility of an empty container and for diamagnetic contributions of the sample by using Pascal's constants.[59] Molecular weights used for magnetic calculations were **1**·1.8 CH_3OH, **2**, **3**, **4**. Fits of the magnetic susceptibility data were performed using PHI[29] using the following Hamiltonian:

$$\hat{H} = \sum D_i[S_{z,i}{}^2 - 1/3S_i(S_i+1) + E_i/D_i(S_{x,i}{}^2 - S_{y,i}{}^2)] + \sum g_{xx,i}\beta\breve{S}_{x,i}\cdot\breve{B}_x + g_{yy,i}\beta\breve{S}_{y,i}\cdot\breve{B}_y + g_{zz,i}\beta\breve{S}_{z,i}\cdot\breve{B}_z$$

Fits of the reduced magnetization data were obtained with the PHI[29] and ANISOFIT 2.0[60] program using a spin Hamiltonian of the form:

$$\hat{H} = D\hat{S}_z{}^2 + E(\hat{S}_x{}^2 + \hat{S}_y{}^2) + g_{iso}\beta\vec{S}\cdot\vec{B}$$

Alternating-current (ac) susceptibility was measured for **1–4** under a 4 Oe ac driving field at frequencies from 1 to 1488 Hz at 1.8 K under applied dc field from 0 to 5000 Oe. The variable temperature ac susceptibility measurements for **1** were performed in the temperature range of 1.8 to 4.6 K under an applied dc field of 2500 Oe.

X-ray structure determinations

All single crystals were coated in Paratone–N oil prior to removal from the glovebox. Data collection was performed by mounting a single crystal on a Cryoloop under a stream of dinitrogen. Data sets were collected targeting complete coverage and fourfold redundancy. Integrations of the raw data were done using the Apex II software package and absorption corrections were applied using SADABS.[61] The structures were solved using direct methods and refined against F^2 using SHELXTL 6.14 software package.[62] Unless otherwise noted, thermal parameters for all non-hydrogen atoms were refined anisotropically. Hydrogen atoms were added at the ideal positions and refined using a riding model in which the isotropic displacement parameters were set at 1.2 times those of the attached carbon atom (1.5 times for methyl carbons).

In the structures of compounds **1**, **2**, and **3**, one of the charge-balancing anions appears to be highly disordered over several locations within an apparent void space. The addition of disordered solvent molecules further complicates modeling of the disordered anion. Several attempts to explicitly model the disorder in $P\bar{3}$ did not afford significant improvement to the agreement factors. Additional attempts to model the disorder in the lower symmetry space group $P\bar{1}$ gave similar problems with the disordered anion and solvent. Thus, SQUEEZE was employed to remove the residual electron density due to the second charge balancing anion. The residual electron density per unit cell for **1** was determined to be 70 electrons and 640 Å^3, which would account for two chloride anions and 2 methanol molecules per unit cell. For complex **2**, the void space within the crystal lattice was determined to be 650 Å^3 and 114 electrons per unit cell. This equates to two bromide anions and 2.33 methanol (or molecules per unit cell. Lastly, the void space of complex **3** was determined to be 675 Å^3 and 284 electrons per unit cell. This equates to two iodide anions and 4.2 diethyl ether molecules per unit cell. Considering the crystalized solvents are diethyl ether the residual electron density corresponds to 0.85, 1.04 and 4.24 diethyl ether molecules per unit cell of **1**, **2** and **3**. As in the NMR we detected presence of methanol we are more inclined to the presence of methanol as the cocrystallized solvent. The chemical formulas supplied in Table S1† do not account for the disordered components that were removed *via* SQUEEZE. Full crystallographic information for **1–4** has been deposited with the CCDC under registry numbers 1030387–1030390.†

Other physical methods

Infrared spectra were measured with a Nicolet 380 FT-IR under a dinitrogen flow using an ATR attachment with a ZnSe crystal. Visible absorption spectra were obtained using an Agilent 8453 UV-visible spectrometer under air-free conditions using a quartz cuvette. ^{1}H NMR spectra were recorded using Varian INOVA instruments operating at 400 MHz. Paramagnetic spectra were acquired at room temperature collecting 512 scans in a spectral window from −22.5 to 200 ppm using an acquisition time of 1 second and a 1 ms relaxation delay. Mass spectra were obtained on a Finnigan LCQ Duo mass spectrometer equipped with an electrospray ion source and quadrupole ion trap mass analyzer in positive ion mode. Elemental analysis was performed by Robertson Microlit Laboratories in Ledgewood, NJ.

Synthesis of Co complex salts

Caution! Perchlorate salts are potentially explosive and should be handled with care and in small quantities!

[CoL$^{5\text{-ONH}t\text{Bu}}$]Cl$_2$ (1). To a suspension of $CoCl_2$ (18 mg, 0.14 mmol) in MeOH (4.5 mL) was added L$^{5\text{-ONH}t\text{Bu}}$ (96 mg, 0.14 mmol) in MeOH (4.5 mL). The resulting orange mixture was stirred at 23 °C for 16 hours to ensure full dissolution of $CoCl_2$. The solution was then concentrated to a volume of 2 mL *in vacuo* and diffraction quality crystals were grown by ether diffusion into this concentrated methanolic solution. The crystals were isolated by filtration and washed with diethyl ether (2 × 5 mL) to give **1** (96 mg, 85% yield). **MS** (ESI$^+$): *m*/*z* found: 384.9 ([CoL$^{5\text{-ONH}t\text{Bu}}$])$^{2+}$, 768.4 ([CoL$^{5\text{-ONH}t\text{Bu}}$–H])$^+$, 804.3 ([CoL$^{5\text{-ONH}t\text{Bu}}$]Cl)$^+$. **^{1}H NMR** (400 MHz, CD_3CN): δ 180, 135, 108, 53, 43, 13, −1.0, −1.3, −16. **UV-Vis** (CH_3CN) λ_{max}/nm (ε_M/M^{-1} cm^{-1}) 234 (56 400), 292, (43 100), 373 (2800), 450 (sh, 650), 510 (sh, 240), 906 (10). Anal calc'd for $C_{40.8}H_{61.2}Cl_2CoN_{10}O_{4.8}$ (**1**·1.8 CH_3OH – methanol was observed in the ^{1}H NMR spectrum): C, 54.54; H, 6.87; N, 15.59. Found: C, 54.35; H, 6.77; 15.80.

[CoL$^{5\text{-ONH}t\text{Bu}}$]Br$_2$ (2). To a solution of L$^{5\text{-ONH}t\text{Bu}}$ (43 mg, 0.060 mmol) in MeOH (3 mL) was added $CoBr_2$ (12 mg, 0.054 mmol) in MeOH (3 mL) and the resulting orange mixture was stirred at 23 °C for 16 hours. The reaction volume was then concentrated *in vacuo* to ∼3 mL and diffraction quality crystals were grown by ether diffusion into this methanolic solution. The crystals were isolated by filtration and washed with diethyl ether (2 × 5 mL) to give **2** (45 mg, 90% yield). **MS** (ESI$^+$): *m*/*z* found: 384.8 ([CoL$^{5\text{-ONH}t\text{Bu}}$])$^{2+}$, 848.3

([$CoL^{5\text{-}ONHtBu}$]Br)$^+$. **^{1}H NMR** (400 MHz, CD_3CN): δ 181, 136, 109, 53, 43, 13, −0.6, −0.8, −15. **UV-Vis** (CH_3CN) λ_{max}/nm (ε_M/M^{-1} cm^{-1}) 220 (sh, 45 600), 240 (sh, 35 000), 287 (24 600), 369 (2900) 450 (sh, 675), 510 (sh, 250), 902 (10). Anal calc'd for $C_{40}H_{61.5}Br_2CoN_{10}O_{5.75}$ (**2**·1 CH_3OH·1.75 H_2O – these solvents were observed in the ^{1}H NMR spectrum): C, 48.36; H, 6.19; N, 14.11. Found: C, 48.37; H, 6.24; N, 14.10.

[$CoL^{5\text{-}ONHtBu}$]I_2 (3). To a solution of $L^{5\text{-}ONHtBu}$ (54 mg, 0.08 mmol) in MeOH (3 mL) was added a solution of CoI_2 (12 mg, 0.08 mmol) in MeOH (10 mL) and the resulting orange mixture was stirred at 23 °C for 1 hour. The reaction volume was then concentrated to ∼3 mL *in vacuo* and diffraction quality crystals were grown by ether diffusion into this methanolic solution. The crystals were isolated by vacuum filtration and washed with diethyl ether (2 × 5 mL) to give **3** (73 mg, 94% yield). **MS** (ESI^+): *m*/*z* found: 384.8 ([$CoL^{5\text{-}ONHtBu}$])$^{2+}$, 769.5 ([$CoL^{5\text{-}ONHtBu}$]H)$^+$, 896.3 ([$CoL^{5\text{-}ONHtBu}$]I)$^+$. **^{1}H NMR** (400 MHz, CD_3CN): δ 178, 148, 108, 52, 44, 13, 2.3, 0.0, −13. **UV-Vis** (CH_3CN) λ_{max}/nm (ε_M/M^{-1} cm^{-1}) 287 (35 500), 370 (4000), 450 (sh, 900), 510 (sh, 360) 908 (10). Anal calc'd for $C_{40}H_{59}I_2CoN_{10}O_{4.5}$ (**3**·1 CH_3OH·0.5 H_2O – methanol and water are observed in the ^{1}H NMR spectrum): C, 45.12; H, 5.59; N, 13.16. Found: C, 44.89; H, 5.44; N 13.24.

[$CoL^{5\text{-}ONHtBu}$]$(ClO_4)_2$ (4). To a solution of $L^{5\text{-}ONHtBu}$ (150 mg, 0.21 mmol) in MeOH (10 mL) was added a solution of $Co(ClO_4)_2$·$6H_2O$ (81 mg, 0.22 mmol) in MeOH (5 mL) and the resulting orange mixture was stirred at 23 °C for 16 hours. The reaction volume was then concentrated to ∼3 mL *in vacuo* and diffraction quality crystals were grown by ether diffusion into this methanolic solution. The crystals were isolated by vacuum filtration and washed with diethyl ether (2 × 5 mL) to give **4** (204 mg, 90% yield). **MS** (ESI^+): *m*/*z* found: 384.8 ([$CoL^{5\text{-}ONHtBu}$])$^{2+}$, 868.4 ([$CoL^{5\text{-}ONHtBu}$](ClO_4))$^+$. **^{1}H NMR** (400 MHz, CD_3CN): δ 177, 160, 108, 51, 44, 13, 4, 0.2, 12. **UV-Vis** (CH_3CN) λ_{max}/nm (ε_M/M^{-1} cm^{-1}) 237 (31 000), 287 (25 400), 373 (3200), 450 (sh, 750), 510, (sh, 260), 900 (10). Anal calcd for $C_{39}H_{54}Cl_2CoN_{10}O_{11}$: C, 48.35; H, 5.62; N, 14.46. Found: C, 48.49; H, 5.78; 14.46.

Synthesis of aldehyde 9 (from which $L^{5\text{-}ONHtBu}$ is derived)

Monoester 6. To a suspension of 2,5-pyridinedicarboxylic acid (**5**, 5.68 g, 34.0 mmol) in MeOH (200 mL, 0.17 M) was added concentrated aqueous H_2SO_4 (5.0 mL, 0.0028 mmol) and the resulting mixture was heated to a gentle boil (∼70 °C). When the reaction became transparent, it was poured on ice and filtered. The precipitate was dissolved in wet THF (100 mL), dried over $MgSO_4$, filtered and concentrated *in vacuo* to isolate crude **6**. The crude compound was then dried overnight in a vacuum oven at 100 °C to give monoester **6** (4.65 g, 75% yield) as a pink solid. **^{1}H NMR** (400 MHz, CD_3OD): δ 9.21 (d, J = 1.6 Hz, 1H), 8.54 (dd, J = 8.0 Hz, 1.6 Hz, 1H), 8.25 (d, J = 8.0 Hz, 1H), 4.01 (s, 3H).

Amide 7. To a suspension of monoester **6** (4.63 g, 25.5 mmol) in anhydrous toluene (80 mL, 0.32 M) was added dropwise freshly distilled (from quinoline) $SOCl_2$ (5.57 mL, 76.6 mmol) and the resulting mixture heated to reflux (∼120 °C). Upon complete conversion to the acyl chloride (visually determined as when the reaction turns transparent yellow), excess $SOCl_2$ and solvent were removed by vacuum distillation to give the crude acid chloride. This residue was then redissolved in anhydrous Et_2O (160 mL, 0.16 M) and cooled to 0 °C, and *tert*-butyl amine (10.74 mL, 102.2 mmol) was added dropwise. The amide formation was immediate as evidenced by precipitation of the amine hydrochloride salt. The reaction was allowed to warm to 23 °C and stirred for 1 h. The mixture was filtered and the precipitate washed with CH_2Cl_2 (2 × 100 mL). The combined filtrates were concentrated *in vacuo* to give crude amide **7** (R_f = 0.61 in EtOAc). This material was used without further purification. **^{1}H NMR** (400 MHz, $CDCl_3$): δ 9.01 (s, 1H), 8.18 (s, 2H), 5.94 (br s, 1H), 4.03 (s, 3H), 1.50 (s, 9H).

Alcohol 8. To a solution of amide **7** (25.5 mmol assumed) in 2 : 1 MeOH : THF (426 mL, 0.06 M) at 0 °C was added anhydrous $CaCl_2$ (8.50 g, 76.6 mmol) and $NaBH_4$ (2.90 g, 76.6 mmol), the latter added portionwise so as to control H_2 evolution. The reaction was allowed to warm to 23 °C and stir overnight. Upon complete consumption of the starting material (as indicated by TLC), the reaction was filtered and concentrated *in vacuo* to give crude alcohol **8**. This residue was purified by flash column chromatography (CH_2Cl_2 to 19 : 1 CH_2Cl_2/MeOH gradient) to give alcohol **8** as a hygroscopic white solid (4.491 g, 85% yield over three steps). **^{1}H NMR** (400 MHz, CD_3OD): δ 8.82 (s, 1H), 8.18 (d, J = 8.0 Hz), 7.62 (d, J = 8.0 Hz, 1H), 4.73 (s, 2H), 1.46 (s, 9H).

Aldehyde 9. To a suspension of alcohol **8** (0.980 g, 4.69 mmol) in 1,4-dioxane (24 mL, 0.20 M) was added SeO_2 (0.260 g, 2.34 mmol) and the resulting mixture was heated to a gentle reflux (∼101 °C) overnight. After allowing to cool to 23 °C, the reaction was filtered through Celite and the filtrate was concentrated *in vacuo* to give crude aldehyde **9**. The crude product was purified by flash column chromatography (1 : 1 hexanes/EtOAc eluent) to afford pure **9** (0.730 g, 75% yield, R_f = 0.44 in 1 : 1 hexanes/EtOAc). **^{1}H NMR** (400 MHz, $CDCl_3$): δ 10.12 (s, 1H), 9.07 (d, J = 1.2 Hz, 1H), 8.20 (dd, J = 8.0, 1.2 Hz, 1H), 8.01 (d, J = 8.0 Hz, 1H), 5.96 (br s, 1H), 1.51 (s, 9H).

Conflicts of interest

There are no conflicts of interest to declare.

Acknowledgements

This work is supported by NSF (CHE-1363274, CHE-1800554) and Colorado State University. We thank R. F. Higgins for assistance with figure preparation.

Notes and references

1 H.-H. Cui, J. Wang, X.-T. Chen and Z.-L. Xue, *Chem. Commun.*, 2017, **53**, 9304–9307.

2 X. Feng, C. Mathonière, I.-R. Jeon, M. Rouzières, A. Ozarowski, M. L. Aubrey, M. I. Gonzalez, R. Clérac and J. R. Long, *J. Am. Chem. Soc.*, 2013, **135**, 15880–15884.
3 C. Mathonière, H.-J. Lin, D. Siretanu, R. Clérac and J. M. Smith, *J. Am. Chem. Soc.*, 2013, **135**, 19083–19086.
4 S. Mossin, B. L. Tran, D. Adhikari, M. Pink, F. W. Heinemann, J. Sutter, R. K. Szilagyi, K. Meyer and D. J. Mindiola, *J. Am. Chem. Soc.*, 2012, **134**, 13651–13661.
5 L. Chen, J. Song, W. Zhao, G. Yi, Z. Zhou, A. Yuan, Y. Song, Z. Wang and Z.-W. Ouyang, *Dalton Trans.*, 2018, **47**, 16596–16602.
6 F. Habib, J. Long, P.-H. Lin, I. Korobkov, L. Ungur, W. Wernsdorfer, L. F. Chibotaru and M. Murugesu, *Chem. Sci.*, 2012, **3**, 2158.
7 S. Zhang, H. Ke, L. Sun, X. Li, Q. Shi, G. Xie, Q. Wei, D. Yang, W. Wang and S. Chen, *Inorg. Chem.*, 2016, **55**, 3865–3871.
8 Q. Chen, M.-H. Zeng, L.-Q. Wei and M. Kurmoo, *Chem. Mater.*, 2010, **22**, 4328–4334.
9 T. J. Woods, M. F. Ballesteros-Rivas, S. Gómez-Coca, E. Ruiz and K. R. Dunbar, *J. Am. Chem. Soc.*, 2016, **138**, 16407–16416.
10 J. Vallejo, E. Pardo, M. Viciano-Chumillas, I. Castro, P. Amorós, M. Déniz, C. Ruiz-Pérez, C. Yuste-Vivas, J. Krzystek, M. Julve, F. Lloret and J. Cano, *Chem. Sci.*, 2017, **8**, 3694–3702.
11 X. Zhang, V. Vieru, X. Feng, J.-L. Liu, Z. Zhang, B. Na, W. Shi, B.-W. Wang, A. K. Powell, L. F. Chibotaru, S. Gao, P. Cheng and J. R. Long, *Angew. Chem., Int. Ed.*, 2015, **54**, 9861–9865.
12 J. Vallejo, F. R. Fortea-Perez, E. Pardo, S. Benmansour, I. Castro, J. Krzystek, D. Armentano and J. Cano, *Chem. Sci.*, 2016, **7**, 2286–2293.
13 M. A. Hoselton, L. J. Wilson and R. S. Drago, *J. Am. Chem. Soc.*, 1975, **97**, 1722–1729.
14 M. Seredyuk, A. B. Gaspar, V. Ksenofontov, Y. Galyametdinov, J. Kusz and P. Gütlich, *J. Am. Chem. Soc.*, 2008, **130**, 1431–1439.
15 C. M. Klug, A. M. McDaniel, S. R. Fiedler, K. A. Schulte, B. S. Newell and M. P. Shores, *Dalton Trans.*, 2012, **41**, 12577.
16 A. M. McDaniel, C. M. Klug and M. P. Shores, *Eur. J. Inorg. Chem.*, 2013, 943–950.
17 Y. Y. Zhu, C. Cui, Y. Q. Zhang, J. H. Jia, X. Guo, C. Gao, K. Qian, S. D. Jiang, B. W. Wang, Z. M. Wang and S. Gao, *Chem. Sci.*, 2013, **4**, 1802–1806.
18 V. V. Novikov, A. A. Pavlov, Y. V. Nelyubina, M. E. Boulon, O. A. Varzatski, Y. Z. Voloshin and R. E. P. Winpenny, *J. Am. Chem. Soc.*, 2015, **137**, 9792–9795.
19 Y. Y. Zhu, Y. Q. Zhang, T. T. Yin, C. Gao, B. W. Wang and S. Gao, *Inorg. Chem.*, 2015, **54**, 5475–5486.
20 J. M. Frost, K. L. M. Harriman and M. Murugesu, *Chem. Sci.*, 2016, **7**, 2470–2491.
21 O. Kahn, *Molecular magnetism*, VCH, New York, NY, 1993.
22 S. Gomez-Coca, E. Cremades, N. Aliaga-Alcalde and E. Ruiz, *J. Am. Chem. Soc.*, 2013, **135**, 7010–7018.
23 Y. Peng, T. Bodenstein, K. Fink, V. Mereacre, C. E. Anson and A. K. Powell, *Phys. Chem. Chem. Phys.*, 2016, **18**, 30135–30143.
24 T. J. Ozumerzifon, I. Bhowmick, W. C. Spaller, A. K. Rappe and M. P. Shores, *Chem. Commun.*, 2017, **53**, 4211–4214.
25 A. M. McDaniel, A. K. Rappé and M. P. Shores, *Inorg. Chem.*, 2012, **51**, 12493–12502.
26 M. Seredyuk, M. C. Munoz, V. Ksenofontov, P. Gutlich, Y. Galyametdinov and J. A. Real, *Inorg. Chem.*, 2014, **53**, 8442–8454.
27 S. Alvarez, P. Alemany, D. Casanova, J. Cirera, M. Llunell and D. Avnir, *Coord. Chem. Rev.*, 2005, **249**, 1693–1708.
28 D. Casanova, P. Alemany, J. M. Bofill and S. Alvarez, *Chem. – Eur. J.*, 2003, **9**, 1281–1295.
29 N. F. Chilton, R. P. Anderson, L. D. Turner, A. Soncini and K. S. Murray, *J. Comput. Chem.*, 2013, **34**, 1164–1175.
30 Y. Ma, A.-L. Cheng and E.-Q. Gao, *Dalton Trans.*, 2010, **39**, 3521.
31 We do not aim to overstate a magnetostructural correlation where the anion in the crystal structure differs from the anion in the magnetic study. Notwithstanding, there are no obvious hydrogen-bonding donor groups in the ester-containing complex that may distort the structure upon differential anion-cation interactions, thus it is reasonable to expect similar local geometries for the two complex salts.
32 L. Chen, H.-H. Cui, S. E. Stavretis, S. C. Hunter, Y.-Q. Zhang, X.-T. Chen, Y.-C. Sun, Z. Wang, Y. Song, A. A. Podlesnyak, Z.-W. Ouyang and Z.-L. Xue, *Inorg. Chem.*, 2016, **55**, 12603–12617.
33 R. F. Higgins, B. N. Livesay, T. J. Ozumerzifon, J. P. Joyce, A. K. Rappé and M. P. Shores, *Polyhedron*, 2018, **143**, 193–200.
34 L. Chen, S.-Y. Chen, Y.-C. Sun, Y.-M. Guo, L. Yu, X.-T. Chen, Z. Wang, Z. W. Ouyang, Y. Song and Z.-L. Xue, *Dalton Trans.*, 2015, **44**, 11482–11490.
35 J. Wang, H.-H. Cui, Y.-Q. Zhang, L. Chen and X.-T. Chen, *Polyhedron*, 2018, **154**, 148–155.
36 B. Drahoš, R. Herchel and Z. Trávníček, *Inorg. Chem.*, 2017, **56**, 5076–5088.
37 D. Shao, Y. Zhou, Q. Pi, F.-X. Shen, S.-R. Yang, S.-L. Zhang and X.-Y. Wang, *Dalton Trans.*, 2017, **46**, 9088–9096.
38 R. Ruamps, L. J. Batchelor, R. Guillot, G. Zakhia, A.-L. Barra, W. Wernsdorfer, N. Guihery and T. Mallah, *Chem. Sci.*, 2014, **5**, 3418–3424.
39 W. H. Harman, T. D. Harris, D. E. Freedman, H. Fong, A. Chang, J. D. Rinehart, A. Ozarowski, M. T. Sougrati, F. Grandjean, G. J. Long, J. R. Long and C. J. Chang, *J. Am. Chem. Soc.*, 2010, **132**, 18115–18126.
40 D. E. Freedman, W. H. Harman, T. D. Harris, G. J. Long, C. J. Chang and J. R. Long, *J. Am. Chem. Soc.*, 2010, **132**, 1224–1225.
41 C. Angeli, S. Borini, M. Cestari and R. Cimiraglia, *J. Chem. Phys.*, 2004, **121**, 4043–4049.
42 C. Angeli, R. Cimiraglia, S. Evangelisti, T. Leininger and J.-P. Malrieu, *J. Chem. Phys.*, 2001, **114**, 10252–10264.

43 C. Angeli, R. Cimiraglia and J.-P. Malrieu, *J. Chem. Phys.*, 2002, **117**, 9138–9153.
44 C. Angeli, R. Cimiraglia and J.-P. Malrieu, *Chem. Phys. Lett.*, 2001, **350**, 297–305.
45 P. G. Szalay, T. Müller, G. Gidofalvi, H. Lischka and R. Shepard, *Chem. Rev.*, 2012, **112**, 108–181.
46 A. D. Becke, *J. Chem. Phys.*, 1993, **98**, 5648–5652.
47 R. E. Stratmann, G. E. Scuseria and M. J. Frisch, *J. Chem. Phys.*, 1998, **109**, 8218–8224.
48 D. Ganyushin and F. Neese, *J. Chem. Phys.*, 2013, **138**, 104113.
49 M. Atanasov, D. Ganyushin, D. A. Pantazis, K. Sivalingam and F. Neese, *Inorg. Chem.*, 2011, **50**, 7460–7477.
50 R. Herchel, L. Váhovská, I. Potočňák and Z. Trávníček, *Inorg. Chem.*, 2014, **53**, 5896–5898.
51 Y. Z. Zhang, S. Gomez-Coca, A. J. Brown, M. R. Saber, X. Zhang and K. R. Dunbar, *Chem. Sci.*, 2016, **7**, 6519–6527.
52 S. Gómez-Coca, A. Urtizberea, E. Cremades, P. J. Alonso, A. Camón, E. Ruiz and F. Luis, *Nat. Commun.*, 2014, **5**, 4300.
53 D. V. Korchagin, G. V. Shilov, S. M. Aldoshin, R. B. Morgunov, A. D. Talantsev and E. A. Yureva, *Polyhedron*, 2015, **102**, 147–151.
54 S. Gómez-Coca, D. Aravena, R. Morales and E. Ruiz, *Coord. Chem. Rev.*, 2015, **289–290**, 379–392.
55 I. Nemec, H. Liu, R. Herchel, X. Q. Zhang and Z. Travnicek, *Synth. Met.*, 2016, **215**, 158–163.
56 C. G. Werncke, E. Suturina, P. C. Bunting, L. Vendier, J. R. Long, M. Atanasov, F. Neese, S. Sabo-Etienne and S. Bontemps, *Chem. – Eur. J.*, 2016, **22**, 1668–1674.
57 M. Pinsky and D. Avnir, *Inorg. Chem.*, 1998, **37**, 5575–5582.
58 L. Gregoli, C. Danieli, A.-L. Barra, P. Neugebauer, G. Pellegrino, G. Poneti, R. Sessoli and A. Cornia, *Chem. – Eur. J.*, 2009, **15**, 6456–6467.
59 G. A. Bain and J. F. Berry, *J. Chem. Educ.*, 2008, **85**, 532.
60 M. P. Shores, J. J. Sokol and J. R. Long, *J. Am. Chem. Soc.*, 2002, **124**, 2279–2292.
61 *APEX 2*, Bruker Analytical X-Ray Systems, Inc., Madison, WI, 2008.
62 G. M. Sheldrick, *SHELXTL, Version 6.14*, Bruker Analytical X-Ray Systems, Madison, WI, 1999.